THE UNIVERSITY OF KANSAS SPACE TECHNOLOGY LABORATORIES
2291 Irving Hill Dr.—Campus West Lawrence, Kansas 66044
Telephone:

PRELIMINARY S-193 RADSCAT OCEANOGRAPHIC DATA FOR SKYLAB II

CRES Technical Memorandum 254-3

Arun Sobti
James Young

February, 1974

Supported by:

NATIONAL AERONAUTICS AND SPACE ADMINISTRATION
Lyndon B. Johnson Space Center
Houston, Texas 77058

CONTRACT NAS 9-13642.

I. INTRODUCTION

The purpose of this report is to disseminate preliminary S-193 RADSCAT oceanography data and associated geographic coordinates for SL-2. These data are necessary to identify the locations where surface and atmospheric truth are needed and to begin preliminary analysis of the microwave returns measured by the S-193.

A total of 12 EREP passes were flown during SL-2. These passes contain 4 segments in which the S-193 was operated in a non-contiguous mode over the sea for more than two or three measurements. These sea measurements are as follows:

EREP#	DOY	START GMT	END GMT	LOCATION
5	156(5 June)	18:02:03	18:08:52	Gulf of Mexico and Caribbean
AVA	157 (6 June)	18:55:31	19:00:31	Hurricane AVA (East of Acapulco)
8	162 (11 June)	15:20:15	15:24:08	Gulf of Mexico
10	164 (13 June)	13:42:01	13:45:45	North Pacific (West of Washington State)

In addition, one cross track contiguous segment was measured on DOY 161 (10 June) along the coast of Brazil. This segment has not been considered in this preliminary analysis since extensive surface truth is not available in that part of the world, and since the CTC mode gives less precision in microwave measurement than do the non-contiguous modes. The data for EREP pass number 10 is also not included in this report since the S-193 was apparently not operating correctly during these sea measurements. The scatterometer signal was much too small and the measured radiometer characteristics are also in error for this segment of EREP pass number 10. The cause of these problems seems to be an inadequate period of warm-up for the S-193 prior to operation.

The data used to produce this report were received from JSC and KSC in the form of tabulations. These tabulations consist of time sequenced voltage recordings for the signal and angle values for pitch and roll. The Housekeeping tabulations were scanned to compute the contributions to the radiometeric temperature from the antenna assembly. The ephemeris information to compute the spatial location

of the target point and the subsatellite point was obtained from the SKYBET print-out contained in the EREP Post Pass Summary Pads.

This report contains tabulations of normalized scattering cross-sections, antenna temperatures, and associated geographical coordinates of the sea segments described previously which were measured during SL-2. Plots of the footprints are also included. The next section describes the algorithms used to generate the data included in this report.

II. CALCULATION PROCEDURES

II.1 Normalized Scattering Cross-Section

From the radar range equation we know that the average received power, P_r, is given by [1]

$$P_r = \frac{P_t \lambda^2}{(4\pi)^3} \iint_{\Omega} \frac{G^2(\theta,\phi)\, A(\theta,\phi,\psi)\, \sigma^\circ(\theta,\phi,\psi)}{R^4(\theta,\phi,\psi)} d\theta d\phi \quad (1)$$

where

ψ = angle of incidence
θ = nadir angle from antenna boresignt
ϕ = azimuth angle w.r.t. antenna boresignt
P_t = transmitted power
λ = wavelength
G = antenna gain
R = range
σ° = normalized scattering cross-section

The underlying assumptions associated with this formulation are understood. In the case of the S-193, the beamwidth of the antenna (two-way) is approximately 1.5° and the normalized scattering cross-section is considered representative over the entire target area. With this assumption, equation (1) can be rearranged as follows:

$$\sigma^\circ(\psi) = \left(\frac{P_r}{P_t}\right) \frac{(4\pi)^3}{\lambda^2} \left(\frac{1}{\iint_{\Omega} \frac{G^2(\theta,\phi)\, A(\theta,\phi,\psi)}{R^4(\theta,\phi,\psi)}\, d\theta d\phi} \right) \quad (2)$$

Equation (2) has been partitioned as shown to illustrate the three effects governing the value of σ°. The first term, $\left(\frac{P_r}{P_t}\right)$, is computed from the voltage recordings on the S-193 tape. To compute this fraction, the system transfer function for a particular mode, incidence angle, filter and gain selection is employed. The second term is a constant because the transmission is at a constant frequency.

The third term is dependent upon the antenna pattern and the target-sensor geometry. With a fixed antenna pattern, the integral is only a function of the target-sensor geometry. It has been shown[2] that a simplified expression for this term provides results accurate to within 0.1 per cent. This expression, shown below, was used in the computation.

$$\frac{1}{\iint_{\Omega} \frac{G^2(\theta,\phi)\,A(\theta,\phi,\psi)}{R^4(\theta,\phi,\psi)}\,d\theta\,d\phi} \cong \frac{R^2}{R_o^2\,I_o}\cos(\alpha)$$

where

R_o = range at nadir angle (height)

I_o = illumination integral $\int \frac{G^2\,A\,dA}{R^4}$ computed for nadir incidence

α = true angle of incidence corrected for earth's curvature.

The value of $R_o^2\,I_o$ was computed apriori and used as a constant (I_g). The value of R_o was estimated as 435 kms. This means that only three values of I_g were stored as constants (the cross polarized values are assumed equal). To adjust for an orbital height other than the nominal 435 kms, a simple correction of the form shown below may be used.

$$I_g' = I_g \frac{R_o'^2}{R_o^2}$$

where I_g' = value of illumination integral for true orbital height R_o'.

A simplified expression to compute α, the true incidence angle used was[3]

$$\alpha = \sin^{-1}\left(\frac{OR}{ER}\sin\gamma\right)$$

where OR = orbital radius

ER = earth's radius

γ = pitch or roll angle of antenna

The range to a target point was computed using the simplified expression[3]

$$R = OR \cdot \cos(\alpha) \left(1 - \sqrt{1 - \left(1 - \frac{ER}{OR}\right)^2 / \cos^2(\alpha)} \right)$$

Having computed the individual entries, the differential backscattering cross-section σ^o was computed as

$$\sigma^o_{(dB)} = 10 \log_{10} \left(\frac{P_r}{P_t} \cdot \frac{R^2 \cos(\alpha)}{I_g} \cdot \frac{(4\pi)^3}{\lambda^2} \right)$$

II.2 Antenna Temperature

The antenna temperature is the sum of all radiometric emissions arriving at the S-193 antenna weighted by the antenna pattern, i.e.

$$T_a = \frac{1}{G_o} \iint T_{app}(\theta, \phi)\, G(\theta, \phi)\, d\theta\, d\phi$$

where

G_o = gain of antenna
T_{app} = apparent temperature
G = antenna pattern
T_a = antenna temperature

The beam efficiency of the antenna is 83.08 per cent for the vertical polarization and 82.55 per cent for the horizontal polarization; the corresponding effective beam widths are 2.00° and 2.06°. Integrating the vertical polarization pattern out to 5° off boresight one finds this solid angle to contain 86.30 per cent of the total energy in the polarization selected and 4.28 per cent of the total energy in the opposite polarization. In other words, the large solid angle from 5 per cent off boresight to 180° contains 9.42 per cent of the total energy. The corresponding figure

for horizontal polarization is 11.05 per cent. The percentage of total energy in the two polarizations with respect to the solid angle off boresight is given in Table 1.

The above mentioned details have been included merely to emphasize that to estimate a surface brightness temperature at antenna boresight merely by examining the antenna temperature can often lead to serious errors. For the case of the ocean, however, a surface distribution of the brightness temperature can often be assumed, thereby allowing one to extract the surface brightness temperature based upon the antenna temperature. Prior to any computation of surface brightness temperature, the effects of the intervening atmosphere must be removed.

The data presented here has not been compensated for atmospheric effects and indeed does not necessarily correspond to the surface brightness temperature in magnitude. It should, however, follow the same trend (although at a different magnitude) as the data measured under carefully controlled and properly compensated recordings.

The S-193 radiometer on board SKYLAB is a modified form of a Dicke Radiometer with two reference temperatures used for internal calibration. The system transfer function accounts for the variations in the two reference voltages and the contributions to the temperature from allintervening hardware elements in the signal path from the antenna to the recorder. For those interested, the system transfer function for the radiometer is contained in G. E.'s Calibration Data Report[5]. The value of the insertion loss of the antenna assembly was computed from data taken over deep space during SL-2.

The gain slope used to convert voltage recordings to degrees Kelvin is found by considering the voltage recordings of two known temperature inputs (the reference temperatures). Due to the random, noise-like nature of the calibration signals, a running average of many calibration recordings was used to compute the gain slope. This is the only deviation from the transfer function proposed by G. E. used for the calculation of antenna temperatures.

TABLE 1

ASSUMED S-193 ANTENNA PATTERN ENERGY DISTRIBUTION

ONE-WAY BEAM EFFICIENCIES

α	VERTICAL POLARIZATION		HORIZONTAL POLARIZATION	
	DOMINANT	CROSSED	DOMINANT	CROSSED
1°	54.20	0.43	53.30	0.30
2°	82.10	2.25	81.14	1.90
3°	84.82	3.66	83.20	3.58
4°	85.90	4.08	83.56	4.14
5°	86.30	4.28	83.73	4.32
180°	93.10	6.90	90.38	9.62
main beam	83.08	——	82.55	——

TWO-WAY BEAM EFFICIENCIES

α	VERTICAL POLARIZATION		HORIZONTAL POLARIZATION	
	DOMINANT	CROSSED	DOMINANT	CROSSED
1°	84.00	0.01	84.75	0.00
2°	95.70	0.06	97.00	0.04
3°	95.78	0.07	97.06	0.06
4°	95.79	0.07	97.06	0.06
5°	95.79	0.07	97.06	0.06
180°	99.92	0.08	99.93	0.07
main beam	95.76	——	97.06	——

II.3 Spatial Location

The spatial locations of the footprint and the subsatellite point are computed in latitude-longitude by means of a simple circular model of the SKYLAB orbit. The eccentricity of the SKYLAB orbit is actually greater than zero, but is very small. The location of the subsatellite point is computed by considering the simple geometry shown in Figure 1.

The angles Ω_p, f, and i uniquely define the position on a unit sphere. These angles are found in a somewhat different form in the SKYBET printouts contained in the EREP Post Pass Pads.

The angle Ω_p is the right ascension of the ascending node. It is given as the right ascension with respect to a fictitious location of the Vernal Equinox in the SKYBET printout. The right ascension computed therein is with respect to the location of the Greenwich Meridian at 00.00 hours on December 31, 1972. A simple translation of the earths axes in the elapsed time to the epoch time provides the necessary value of the right ascension. The value of i, the inclination angle of the orbit, is listed for one-minute intervals in the SKYBET printout. The value of f, the perifocal angle, is computed by summing the argument of the perigee and the mean anomaly. All the numbers found in the SKYBET document are printed for one minute intervals only. An interpolation scheme computes the values at the precise moments of interest.

Having resolved the unit vector into its three coordinates w.r.t. the x' y' z axis, the latitude is computed by simple geometry. The longitude with respect to the x' axis is similarly computed. A rotation by the amount Ω_p then provides the longitude with respect to the Greenwich Meridian.

The target location is found by computing the unit vector of antenna boresight in terms of the x' y' z coordinate system shown in Figure 1. To do this one must go through many sets of coordinate transformations[3]. These coordinate transformations utilize angles provided in the SKYBET printout. After the unit vector and the range to the target point have been computed, the vector sum of the vehicle position vector and the pointing vector determines the position vector of the target on the face of the earth. This can then be resolved into latitude and longitude.

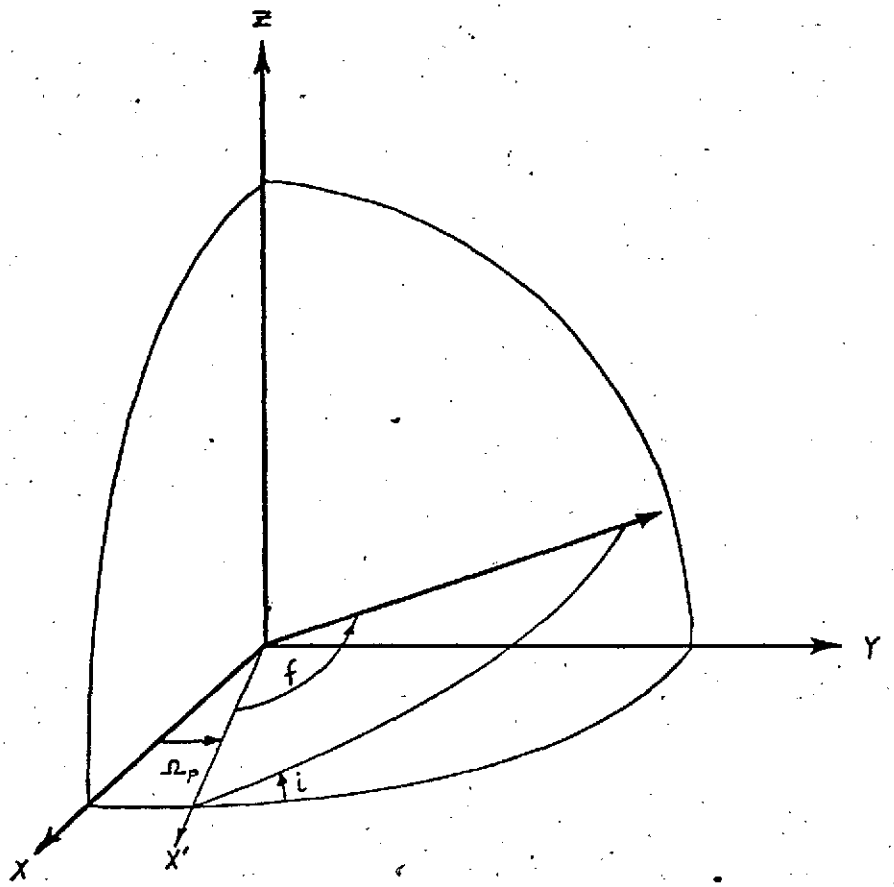

Figure 1. Skylab Orbital Geometry.

The plots were made by encoding a tape to run a Benson-Lehner Incremental Plotter. The accuracy of the location of the center of the footprint as verified by sample printouts (every 20 seconds-for nadir incidence) from EREP Post Pass Pads is within 0.10° longitude and latitude. This accuracy is well within the tolerances of estimating the various attitude and antenna excursions.

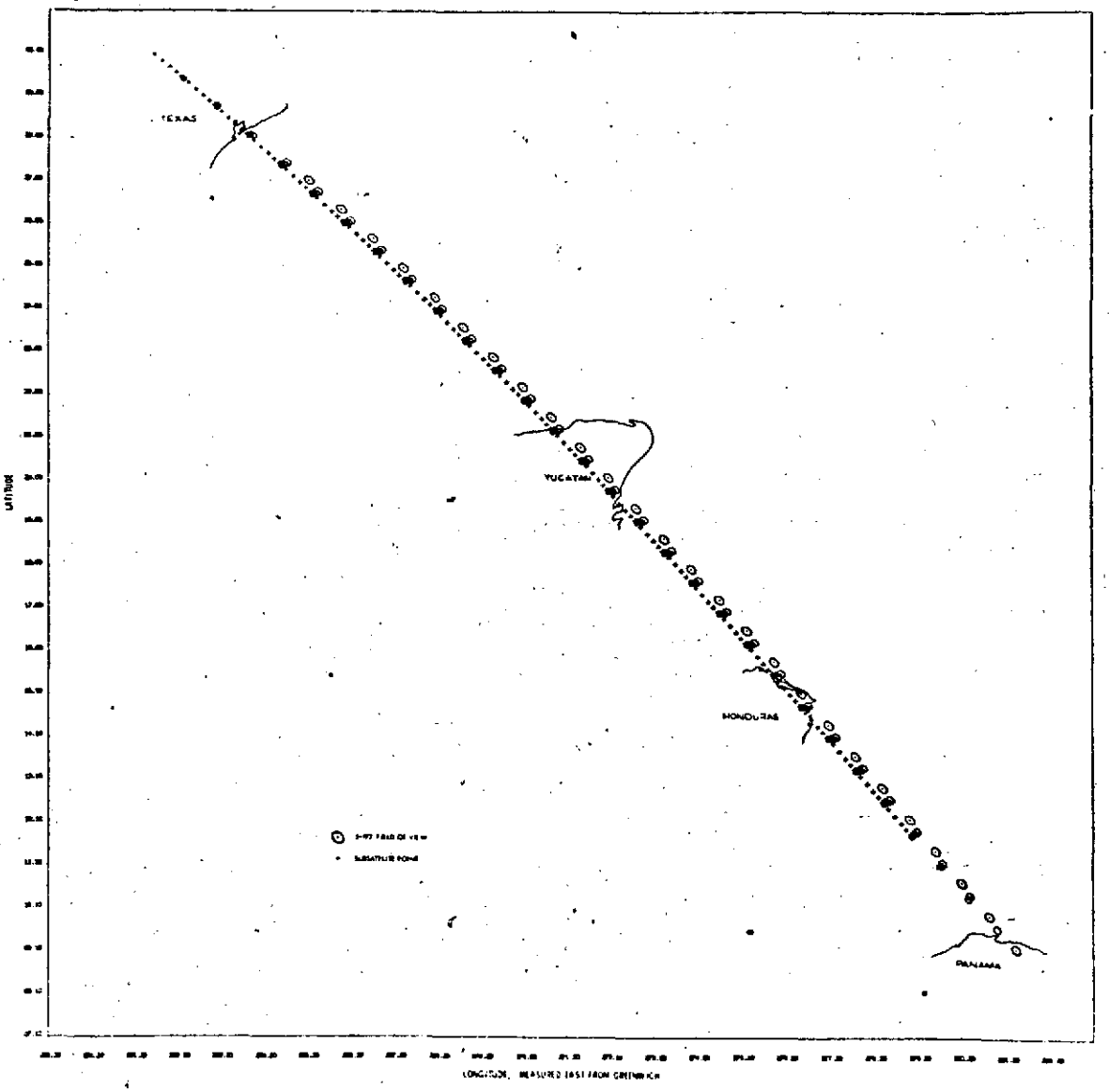

Figure 2. S-193 RADSCAT Coverage on DOY 156 (5 June).

TABLE 2

Preliminary S-193 RADSCAT Data for DOY 156 (5 June).

Scan Numb	GMT (Hr Min Sec)	Angle of Incidence (Deg)	Scattering Coefficients VV (DB)	VH (DB)	HH (DB)	HV (DB)	Antenna Temps V (Deg)	H (Deg)	Field of View Coordinates Lat (Deg)	Long (Deg)	Subsatellite Coordinates Lat (Deg)	Long (Deg)
	18 2 9.33	50.52	-21.47	-33.41	-26.16	-39.48	162.07	100.89	27.38	-94.75	30.23	-98.34
	18 2 12.89	43.84	-17.38	-31.85	-20.60	-32.80	153.65	107.99	27.72	-95.27	30.08	-98.16
1	18 2 16.25	32.38	-13.58	-27.57	-13.99	-27.90	147.89	126.17	28.34	-96.06	29.93	-97.88
	18 2 19.03	17.19	-7.70	-13.90	-7.25	-14.84	283.01	282.57	29.04	-96.83	29.81	-97.35
	18 2 21.33	1.15							29.65	-97.63	29.71	-97.73
	18 2 24.58	50.53	-17.78	-32.19	-23.25	-33.27	163.41	102.67	26.62	-94.02	29.57	-97.97
	18 2 28.14	43.84	-16.18	-32.24	-21.13	-34.79	153.21	107.10	27.04	-94.54	29.42	-97.39
	18 2 31.50	32.38	-13.04	-26.39	-13.74	-27.57	146.07	121.59	27.67	-95.31	29.27	-97.22
2	18 2 34.28	17.19	1.01	-15.26	1.31	-14.66	136.36	130.54	28.37	-96.12	29.15	-97.
	18 2 36.58	1.15	12.32	-4.41	16.63	-6.00	277.53	282.46	28.99	-96.91	28.05	-96.36
	18 2 39.83	50.53	-17.40	-31.78	-22.91	-33.25	162.28	101.85	25.93	-93.38	28.91	-95.50
	18 2 43.39	43.84	-16.34	-31.01	-19.73	-32.29	150.72	105.42	26.36	-93.81	28.75	-95.62
	18 2 46.75	32.38	-13.16	-27.41	-13.45	-27.73	142.60	117.93	26.99	-94.57	28.68	-96.46
3	18 2 49.53	17.19	1.19	-13.98	1.67	-14.49	132.14	125.41	27.70	-95.38	28.48	-95.32
	18 2 51.83	1.15	13.29	-2.31	13.43	-3.73	128.72	125.10	28.32	-96.15	28.38	-96.21
	18 2 55.08	50.53	-16.73	-31.77	-22.73	-32.31	161.13	99.98	25.24	-92.59	28.24	-95.45
	18 2 38.64	43.85	-15.97	-30.31	-19.71	-30.66	149.77	103.66	25.67	-93.09	28.08	-95.27
	18 3 2.00	32.38	-12.05	-26.34	-12.99	-26.84	140.31	116.41	26.31	-93.85	27.93	-95.71
4	18 3 4.78	17.19	0.84	-14.08	1.21	-15.62	130.80	122.69	27.02	-94.64	27.81	-95.57
	18 3 7.08	1.15	12.91	-3.07	13.34	-3.79	126.10	122.50	27.65	-95.41	27.71	-95.46
	18 3 10.33	50.52	-18.88	-33.81	-24.50	-35.16	162.31	99.29	24.55	-91.88	27.56	-95.30
	18 3 13.89	43.84	-16.66	-31.00	-20.15	-31.83	150.02	104.52	24.98	-92.38	27.40	-95.13
	18 3 17.25	32.37	-11.71	-26.10	-12.83	-26.97	140.36	116.81	25.62	-93.13	27.25	-94.97
5	18 3 20.03	17.17	1.36	-14.78	1.33	-14.47	130.34	123.11	26.34	-93.91	27.13	-94.83
	18 3 22.33	1.14	13.61	-2.69	13.69	-3.53	124.29	122.95	26.97	-94.67	27.03	-94.72
	18 3 25.58	50.52	-20.92	-34.18	-26.07	-37.18	159.70	98.66	23.85	-91.19	26.88	-94.57
	18 3 29.14	43.83					406.25	104.42	24.29	-91.68	26.72	-94.45
6	18 3 32.50	32.36					141.95	118.44	24.93	-92.42	25.57	-94.34
	18 3 35.28	17.16	1.13	-14.88	1.54	-14.42	129.95	123.15	25.65	-93.19	25.45	-94.13
	18 3 37.58	1.13	13.16	-3.23	13.17	-3.85	122.81	122.36	26.29	-93.95	25.35	-94.00
	18 3 46.83	50.50	-20.76	-33.60	-25.92	-37.17	159.00	97.96	23.15	-90.50	26.20	-93.34
	18 3 44.39	43.82	-19.37	-33.26	-22.37	-33.91	148.00	102.81	23.59	-90.99	26.04	-93.67
7	18 3 47.75	32.35	-13.60	-27.38	-14.64	-28.21	139.05	116.45	24.24	-91.72	25.89	-93.52
	18 3 50.53	17.15	0.96	-14.66	1.52	-15.47	130.62	122.93	24.36	-92.49	25.76	-93.
	18 3 52.83	1.11	13.20	-3.28	13.47	-4.05	124.03	122.22	25.60	-93.23	25.66	-93.2
	18 3 56.08	50.49	-20.03	-31.87	-25.91	-36.49	159.41	98.78	22.45	-89.82	25.51	-93.1
	18 3 59.64	43.81	-18.60	-32.15	-21.93	-33.99	147.62	101.82	22.89	-90.30	25.35	-92.96
8	18 4 3.00	32.34	-13.52	-28.21	-14.19	-28.40	137.85	116.11	23.54	-91.03	25.20	-92.30
	18 4 5.78	17.15	0.75	-14.97	1.21	-14.73	128.79	121.09	24.27	-91.79	25.97	-92.67
	18 4 8.08	1.11	13.35	-3.10	13.26	-3.90	123.10	121.75	24.91	-92.52	24.97	-92.57

TABLE 2 (Continued) (DOY 156).

Scan Numb	GMT (Hr Min Sec)	Angle of Incidence (Deg)	Scattering Coefficients VV (DB)	VH (DB)	HH (DB)	HV (DB)	Antenna Temps V (Deg)	H (Deg)	Field of View Coordinates Lat (Deg)	Long (Deg)	Subsatellite Coordinates Lat (Deg)	Long (Deg)
	18 6 13.33	50.48	-15.26	-27.58	-16.55	-28.36	174,05	140.14	15.96	-84.00	18.15	-87.05
	18 6 16.89	43.79	-14.02	-26.99	-17.69	-27.64	155.52	112.57	16.42	-84.45	18.99	-86.90
17	18 6 20.25	32.32	-11.33	-24.15	-12.16	-24.78	148.66	127.90	17.10	-85.13	18.43	-85.76
	18 6 23.03	17.12	0.64	-14.45	1.17	-14.96	134,37	132.57	17.85	-85.82	18.70	-86.84
	18 6 25.33	1.08	13.41	-3.72	13.29	-4.06	123,84	126.09	18.53	-86.50	18.59	-86.54
	18 6 28.58	50.47	-14.98	-26.37	-19.59	-27.17	176,19	117.07	15.23	-83.39	18.43	-86.41
	18 6 32.14	43.78	-13.42	-27.01	-16.92	-27.64	157,24	113.36	15.69	-83.83	18.20	-86.26
18	18 6 35.50	32.31	-10.75	-24.45	-12.21	-24.53	147,23	124.12	16.37	-84.50	18.18	-86.12
	18 6 38.28	17.11	1.23	-14.08	1.55	-14.47	135,65	127.51	17.13	-85.19	17.97	-86.00
	18 6 40.58	1.06							17.80	-85.87	17.86	-85.91
	18 6 43.83	50.46	-15.60	-28.46	-20.77	-29.02	165,42	106.20	14.49	-82.78	17.71	-85.77
	18 6 47.39	43.77	-12.29	-20.74	-14.56	-24.91	158,70	126.38	14.36	-83.22	17.54	-85.63
19	18 6 50.75	32.30	-9.85	-23.35	-10.81	-23.66	147,52	124.78	15.64	-83.88	17.38	-86.43
	18 6 53.53	17.10	0.73	-14.91	1.47	-14.44	134.70	128.78	16.40	-84.57	17.25	-85.37
	18 6 55.33	1.05	12.79	-3.91	12.64	-4.42	126.66	125.74	17.08	-85.24	17.14	-85.28
	18 6 59.08	50.45	-16.32	-29.22	-21.62	-29.99	163,08	105.66	13.76	-82.17	16.98	-85.14
	18 7 2.64	43.76	-14.52	-26.99	-17.95	-27.61	153,93	106.92	14.22	-82.61	16.81	-85.00
20	18 7 6.00	32.29	-9.63	-16.57	-10.00	-21.91	152,70	157.25	14.98	-83.27	16.65	-84.86
	18 7 8.78	17.09	1.55	-14.58	1.62	-15.04	137,56	130.31	15.67	-83.95	16.52	-84.75
	18 7 11.08	1.04	12.94	-3.93	12.90	-4.50	127,78	128.23	16.35	-84.61	16.41	-84.65
	18 7 14.33	50.44	-17.00	-29.14	-21.85	-29.99	164,19	107.01	13.02	-81.56	16.25	-84.52
	18 7 17.89	43.75	-15.54	-27.61	-18.34	-27.97	154,52	111.61	13.48	-82.00	16.08	-84.37
21	18 7 21.25	32.28	-10.77	-23.78	-11.96	-24.43	147,45	123.58	14.17	-82.66	15.92	-84.24
	18 7 24.03	17.03	-3.03	-12.84	-1.10	-14.37	174,49	204.21	14.94	-83.33	15.79	-84.12
	18 7 25.33	1.03	12.60	-4.11	12.97	-4.59	140,78	134.93	15.62	-83.99	15.68	-84.03
	18 7 29.58	50.43	-17.78	-29.99	-22.28	-31.12	165,98	110.75	12.28	-80.97	15.52	-83.90
	18 7 33.14	43.74	-15.67	-27.57	-18.50	-28.53	136,10	113.00	12.76	-81.40	15.35	-83.76
22	18 7 36.50	32.27	-11.08	-24.20	-11.82	-24.13	146,53	124.96	13.43	-82.05	15.19	-83.62
	18 7 39.28	17.07	1.36	-13.91	1.57	-15.67	136,60	123.97	14.20	-82.72	15.05	-83.51
	18 7 41.58	1.02	15.23	0.31	16.77	-4.03	134,08	193.86	14.39	-83.38	14.94	-83.42
	18 7 44.83	50.42	-14.25	-30.13	-22.80	-30.13	168,67	113.47	11.54	-80.37	14.79	-83.29
	18 7 48.39	43.73	-15.53	-27.79	-18.69	-28.13	136,91	115.50	12.00	-80.80	14.63	-83.14
23	18 7 51.75	32.26	-11.07	-24.19	-11.88	-24.34	147,50	125.00	12.69	-81.45	14.45	-83.01
	18 7 54.53	17.05	1.37	-14.77	1.46	-14.11	135,52	130.58	13.47	-82.12	14.32	-82.98
	18 7 56.83	1.01	12.94	-4.11	12.60	-4.32	131,37	130.03	14.15	-82.77	14.21	-82.81
	18 8 0.08	50.41	-20.92	-32.05	-24.81	-35.05	167,47	110.86	10.80	-79.78	14.05	-82.68
	18 8 3.64	43.72	-16.47	-28.47	-19.75	-29.19	157,72	115.41	11.26	-80.20	13.87	-82.53
24	18 8 7.00	32.25	-11.29	-24.41	-12.35	-24.41	148,45	128.21	11.94	-80.85	13.71	-82.39
	18 8 9.78	17.05	1.50	-14.78	1.68	-14.26	138,15	130.50	12.72	-81.51	13.57	-82.28
	18 8 12.08	1.00	12.41	-4.39	12.41	-5.01	128,25	128.25	13.40	-82.15	13.45	-82.19

TABLE 2 (Continued) (DOY 156).

Scan Numb	GMT (Hr Min Sec)	Angle of Incidence (Deg)	Scattering Coefficients VV (DB)	VH (DB)	HH (DB)	HV (DB)	Antenna Temps V (Deg)	H (Deg)	Field of View Coordinates Lat (Deg)	Long (Deg)	Subsatellite Coordinates Lat (Deg)	Long (Deg)
	18 8 15.33	50.40	-19.82	-29.27	-16.17	-27.12	197.58	142.75	10.03	-79.17	13.29	-82.05
	18 8 18.89	43.71	-20.23	-32.05	-22.50	-33.30	160.93	118.74	10.49	-79.59	13.12	-81.91
25	18 8 22.25	32.24	-12.50	-25.08	-13.14	-25.67	147.79	126.02	11.18	-80.23	12.95	-81.77
	18 8 25.63	17.64	1.24	-14.89	1.53	-14.33	136.21	131.26	11.95	-80.89	12.81	-81.66
	18 8 27.33	0.99	12.38	-4.55	12.40	-4.88	132.16	133.05	12.44	-81.53	12.69	-81.57
	18 8 30.58	50.39	-6.82	-13.94	-6.24	-14.12	260.83	246.44	9.27	-78.57	12.53	-81.43
	18 8 34.14	43.70	-13.50	-24.62	-12.88	-25.97	192.91	178.07	9.73	-78.99	12.36	-81.29
26	18 8 37.50	32.23	-13.68	-27.28	-14.57	-27.28	134.66	129.90	10.42	-79.62	12.19	-81.15
	18 8 40.28	17.03	1.03	-14.30	1.21	-14.69	138.46	132.61	11.19	-80.28	12.05	-81.04
	18 8 42.57	0.98	12.32	-4.36	12.09	-4.88	130.33	130.80	11.88	-80.92	11.93	-80.95

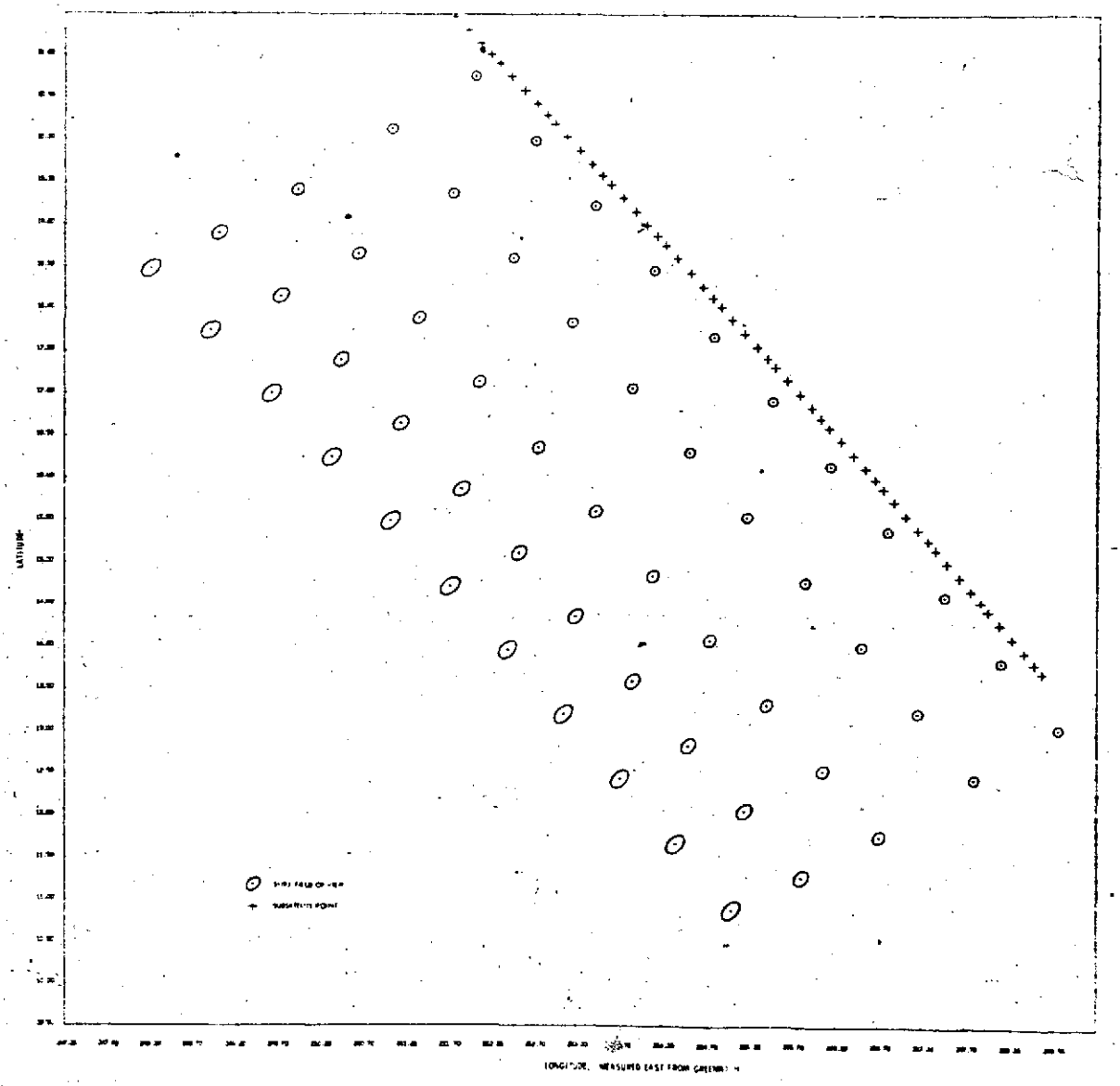

Figure 3. S-193 RADSCAT Coverage on DOY 157 (6 June).

TABLE 3

Preliminary S-193 RADSCAT Data for DOY 157 (6 June).

Scan Numb	GMT (Hr Min Sec)	Angle of Incidence (Deg)	Scattering Coefficients VV (DB)	VH (DB)	HH (DB)	HV (DB)	Antenna Temps. H (Deg)	V (Deg)	Field of View Coordinates Lat (Deg)	Long (Deg)	Subsatellite Coordinates Lat (Deg)	Long (Deg)
	18 55 58.84	51.60	-16.17	-29.00	-25.48	-30.72	108.06	163.46	18,48	111.78	21.47	108.23
	18 56 2.40	45.15	-18.38	-31.05	-23.35	-31.10	112.45	154.19	18,21	110.97	21.31	108.06
1	18 56 5.76	35,87	-17.33	-30.61	-20.28	-31,00	123.38	147.73	19,42	110.06	21.15	107.93
	18 56 8.54	20,57	-6.54	-21.81	-7.82	-21.86	131.91	139.20	20.14	108.96	21.02	107.81
	18 56 10.84	4,65	13.25	-2.86	12.43	-3.02	131.50	133.48	20,76	108,00	20.91	107.71
	18 56 14.09	51,57	-16.79	-28,71	-24,00	-30.42	112.45	166.28	17,75	111.07	20.76	107.57
	18 56 17.65	45,11	-16.10	-29,64	-22.49	-31,12	115.94	156.95	18,16	110.26	20.60	107.42
2	18 56 21.01	35,83	-15.97	-29.34	-13.76	-29.63	126.48	149.65	18,67	109.35	20.44	107.28
	18 56 23.79	20,52	-3.12	-18,87	-2.67	-18,39	134.32	142.47	19,38	108,25	20.31	107.16
	18 56 26,09	4,52	14.09	-3,47	13,79	-2,76	133.06	133.06	20,00	107,29	20.20	107.06
	18 56 29.34	51,55	-16.33	-28,95	-23.89	-30,45	114.81	168.46	17,01	110.36	20.05	106.92
	18 56 32.90	45,10	-14.73	-28,18	-20.56	-29,10	117.29	159.19	17,41	109.55	19.89	106.77
3	18 56 36.26	35,82	-13.56	-27,05	-13.99	-27,39	127.96	151.98	17,91	108.65	19.73	106.62
	18 56 39,04	20,52	-2,12	-17,50	-2,74	-17,09	135.45	143.21	18,62	107.55	19.60	106.50
	18 56 41.34	4,64	13,09	-4,28	12,95	-3,82	133.44	135.03	19,24	106,59	19.49	106.41
	18 56 44.59	51,55	-14.51	-27,55	-21,69	-28,50	115.73	170.46	16,25	109,66	19.34	106.27
	18 56 48.15	45,11	-13.30	-27,29	-19,09	-27,48	118.90	159.68	16,66	108.85	19.17	106.12
4	18 56 51.51	35,84	-12.32	-26,19	-14,56	-26,01	129.09	151.98	17,15	107,95	19.01	105,98
	18 56 54.29	20,58	-2,21	-18,16	-2,72	-17,57	134.91	142.69	17,86	106,85	18.88	105.86
	18 56 56.59	4,98	13,22	-4,11	13,02	-3,63	133.53	134.37	18,48	105,49	18.77	105.76
	18 56 59.84	51,57	-13.44	-26,72	-20,32	-27,81	117.93	170.76	15,50	108.97	18.62	105.63
	18 57 3.40	45,14	-12.67	-26,09	-17,86	-27,00	120.45	161.42	15,88	108.15	18.49	105.47
5	18 57 6.76	35,90	-14.93	-26,86	-17,60	-28,40	128.17	151.56	16,38	107,25	18.29	105.33
	18 57 9.54	20,71	-4,18	-17,77	-4,20	-19,33	134.85	143.87	17,08	106.15	18.16	105.21
	18 57 11.84	5,58	12,80	-4,95	12,72	-4,21	133.93	131.86	17,69	105,20	18.05	105.12
	18 57 15.09	51,61	-14.39	-26,07	-13,81	-26,72	120.84	173.42	14,73	108.28	17.90	104.98
	18 57 18.65	45,19	-14.54	-26,56	-17,35	-27,16	121.46	160.91	15,12	107,47	17.73	104.84
6	18 57 22.01	35,98	-12.37	-26,46	-14,69	-26,74	130.24	152.35	15,62	106,57	17.57	104.70
	18 57 24,77	20,88	-3,02	-18,76	-3,65	-18,33	135.12	218.82	16,32	105,48	17.44	104.58
	18 57 27,09	6,23	11,53	-5,68	11,51	-5,01	133.25	132.41	16,93	104,52	17.33	104.49
	18 57 30,34	51,67	-13.61	-25,95	-19,47	-26,85	123.74	173.58	13,97	107,60	17.18	104.35
	18 57 33,90	45,27	-14.51	-28,14	-19,08	-28,14	122.05	161.39	14,56	106,60	17.01	104.21
7	18 57 37,26	36,08	-13.12	-26,61	-14,31	-26,31	132.69	154.41	14,85	105,90	16.85	104.87
	18 57 40,04	21,09	-3,14	-18,92	-3,21	-18,51	139.43	144.96	15,55	104,81	16.72	103.96
	18 57 42.34	6,98	11,20	-6,22	10,76	-5,61	136.25	133.41	16,16	103,85	16.61	103.86
	18 57 45,59	51,74	-12.64	-22,02	-15,73	-22,38	145.03	188.17	13,20	106,94	16.46	103.73
	18 57 49,15	45,36	-14.66	-25,69	-16,14	-25,95	139.89	174.50	13,59	106,14	16.29	103.59
8	18 57 52,51	36,22	-14.58	-27,89	-15,17	-27,89	133.30	155.69	14,08	105,24	16.13	103.45
	18 57 55,29	21,34	-3,14	-19,25	-3,41	-18,59	138.21	145.56	14,78	104,14	16.00	103.34
	18 57 57,59	7,79	9,98	-7,45	9,87	-6,87	135.42	133.83	15,38	103,19	15.89	103.24

TABLE 3 (Continued) (DOY 157).

Scan Numb	GMT (Hr Min Sec)	Angle of Incidence (Deg)	Scattering Coefficients VV (DB)	VH (DB)	HH (DB)	HV (DB)	Antenna Temps. H (Deg)	V (Deg)	Field of View Coordinates Lat (Deg)	Long (Deg)	Subsatellite Coordinates Lat (Deg)	Long (Deg)
	18 58 0.84	51.83	-13.52	-22.67	-15.00	-23.00	152.09	188.77	12.43	106.29	15.74	103.12
	18 58 4.40	45.47	-13.20	-25.50	-16.04	-25.43	134.89	170.53	12.83	105.48	15.57	102.97
9	18 58 7.76	36.37	-15.84	-30.95	-16.80	-30.05	133.36	155.45	13.31	104.58	15.41	102.84
	18 58 10.54	21.65	-6.51	-22.26	-6.13	-21.78	135.54	142.08	14.01	103.49	15.27	102.73
	18 58 12.84	8.64	7.75	-9.41	7.66	-8.69	133.10	133.94	14.61	102.53	15.16	102.63
	18 58 16.09	51.24	-13.43	-22.10	-12.51	-22.26	216.08	233.71	11.66	105.63	15.01	102.50
	18 58 19.65	45.61	-14.53	-27.29	-17.60	-27.84	128.17	165.12	12.05	104.63	14.84	102.36
10	18 58 23.01	36.56	-18.35	-33.26	-20.15	-33.99	140.28	160.34	12.53	103.93	14.68	102.23
	18 58 25.79	21.99	-11.17	-25.84	-11.47	-25.03	137.47	144.01	13.23	102.83	14.55	102.11
	18 58 28.09	9.53	3.04	-13.19	2.67	-12.51	134.92	132.49	13.83	101.88	14.44	102.02
	18 58 31.34	52.06	-16.59	-28.09	-19.16	-28.41	134.63	184.27	10.88	104.99	14.28	101.89
	18 58 34.90	45.76	-18.53	-30.80	-21.15	-31.18	131.54	169.24	11.27	104.18	14.11	101.75
11	18 58 38.26	36.77	-21.24	-33.27	-22.48	-39.54	134.00	154.71	11.75	103.28	13.95	101.62
	18 58 41.04	22.37	-16.25	-30.79	-15.76	-29.92	143.59	153.41	12.45	102.19	13.82	101.51
	18 58 43.34	10.45	-3.07	-17.64	-3.48	-17.14	136.70	135.13	13.05	101.23	13.71	101.42
							145.95	195.02				
							125.18	162.91				
							135.65	155.93				
							142.41	147.65				
							138.06	134.83				
							126.23	175.05				
							123.32	160.76				
							133.10	152.65				
							139.77	143.84				
							137.71	134.05				
							119.53	153.35				
							121.63	159.51				
							132.62	152.60				
							139.02	143.94				
							154.70	146.91				
							117.07	167.50				
							120.50	157.33				
							135.09	154.07				
							193.32	198.61				
							140.42	137.56				
							116.99	167.46				
							120.69	157.21				
							131.35	150.66				
							163.01	167.46				
							141.18	134.20				

18

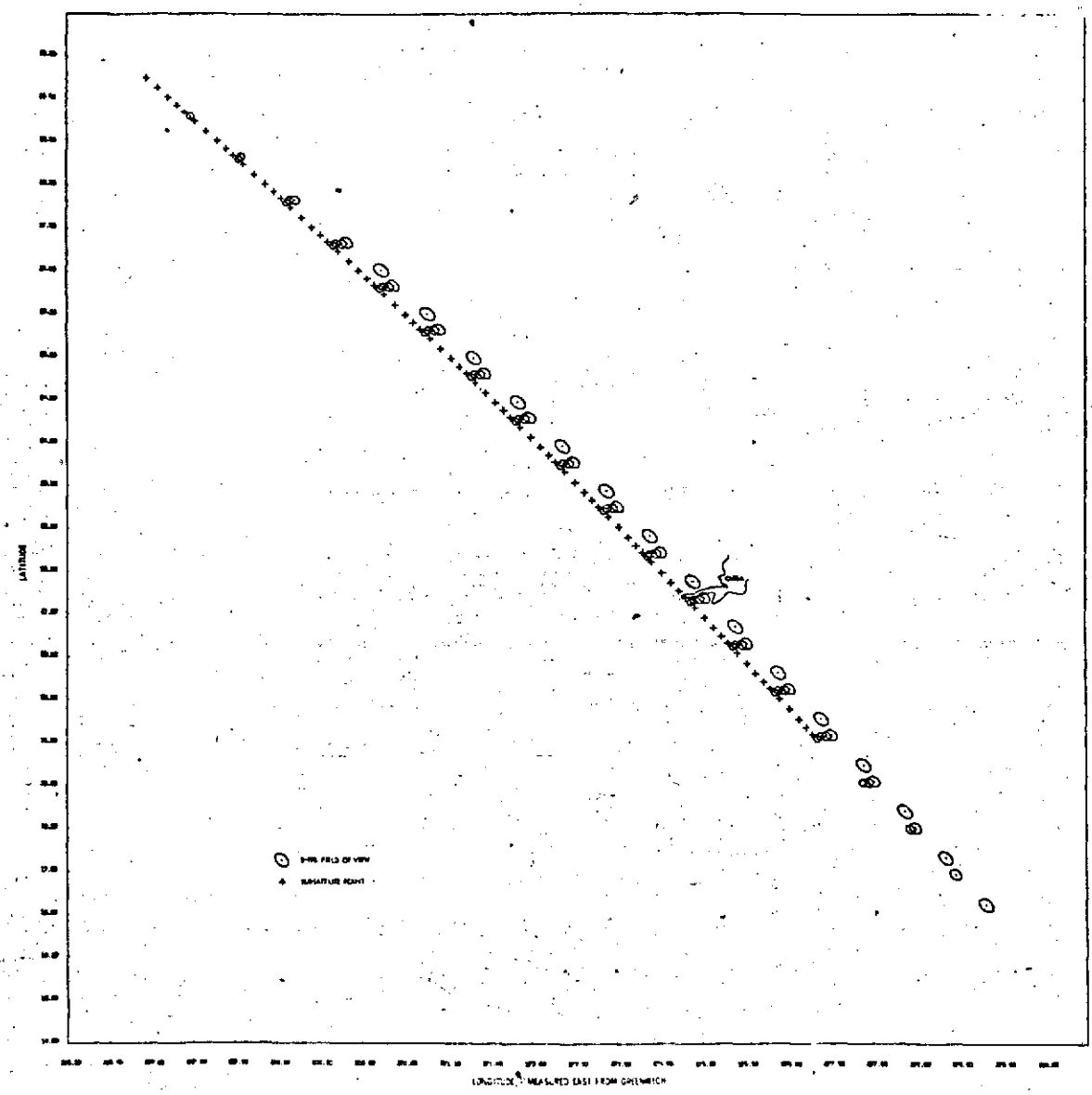

Figure 4. S-193 RADSCAT Coverage on DOY 162 (11 June).

TABLE 4

Preliminary S-193 RADSCAT Data for DOY 162 (11 June).

Scan Numb	GMT (Hr Min Sec)	Angle of Incidence (Deg)	Scattering Coefficients VV (DB)	VH (DB)	HH (DB)	HV (DB)	Antenna Temps V (Deg)	H (Deg)	Field of View Coordinates Lat (Deg)	Long (Deg)	Subsatellite Coordinates Lat (Deg)	Long (Deg)
	15 20 21.44	51.33	-31.03	-35.04	-35.71	-47.85			26.94	89.71	29.90	93.42
	15 20 25.00	44.58	-26.88	-36.20	-29.62	-47.46			27.37	90.25	23.75	93.24
1	15 20 28.36	32.84	-15.63	-28.87	-16.79	-31.33			28.03	91.07	29.60	93.07
	15 20 31.14	17.83	-0.35	-15.06	0.10	-15.78			28.69	91.91	29.48	92.93
	15 20 33.44	1.62							29.32	92.72	29.36	92.81
	15 20 36.69	51.32	-19.37	-33.16	-22.19	-36.88	168.73	118.26	26.26	88.98	29.24	92.65
	15 20 40.25	44.57	-27.32	-35.07	-31.21	-37.73	159.17	113.68	26.76	89.52	29.09	92.47
2	15 20 43.61	32.83	-19.27	-30.58	-19.78	-33.43	151.76	128.80	27.35	90.33	28.94	92.30
	15 20 46.39	17.82	-0.86	-15.51	-0.43	-16.22	143.67	139.70	28.03	91.16	28.82	92.16
	15 20 48.69	1.61	15.14	-1.45	15.13	-2.12	132.76	130.75	28.66	91.95	28.72	92.05
	15 20 51.94	51.31	-23.54	-35.37	-29.52	-38.47	167.75	106.70	25.57	88.26	28.58	91.88
	15 20 55.50	44.57	-22.81	-33.43	-21.26	-37.94	155.71	110.82	26.02	88.80	28.42	91.71
3	15 20 58.86	32.82	-20.52	-31.79	-22.12	-35.04	145.94	121.39	26.68	89.59	28.27	91.54
	15 21 1.64	17.81	-1.44	-16.09	-0.64	4.75	137.58	129.60	27.35	90.42	28.15	91.41
	15 21 3.93	1.59	14.55	-1.66	14.51	-1.98	133.50	133.08	27.99	91.20	28.05	91.29
	15 21 7.19	51.28	-25.51	-34.26	-29.67	-47.86	163.21	103.22	24.89	87.56	27.91	91.13
	15 21 10.75	44.53	-24.06	-34.17	-27.09	-46.49	155.69	110.67	25.33	88.08	27.75	90.96
4	15 21 14.11	32.77	-19.88	-30.58	-17.77	-32.26	146.60	122.87	26.00	89.87	27.60	90.80
	15 21 16.89	17.76	-3.09	-17.77	-2.93	-18.40	133.43	126.63	26.68	89.69	27.48	90.66
	15 21 19.18	1.54	15.36	-0.83	15.23	-1.71	126.63	125.32	27.32	90.46	27.38	90.55
	15 21 22.44	51.23	-24.41	-36.42	-29.09	-47.85	162.09	101.21	24.20	86.86	27.24	90.39
	15 21 26.00	44.48	-22.80	-36.19	-26.17	-37.94	151.83	106.15	24.85	87.38	27.05	90.22
5	15 21 29.36	32.73	-19.27	-32.26	-19.53	-31.78	143.33	118.67	25.32	88.16	26.93	90.06
	15 21 32.14	17.71	-2.47	-16.30	-1.73	-16.88	136.68	125.64	26.00	88.96	26.81	89.92
	15 21 34.43	1.50	15.99	-0.38	15.76	-1.28	124.06	122.28	26.64	89.73	26.76	89.81
	15 21 37.69	51.18	-21.34	-33.53	-26.32	-36.89	161.07	100.63	23.51	86.17	26.56	89.66
	15 21 41.25	44.43	-21.44	-34.18	-24.29	-35.07	150.57	104.21	23.96	86.69	26.40	89.49
6	15 21 44.61	32.68	-15.93	-29.94	-16.70	-31.34	141.09	117.40	24.63	87.46	26.25	89.33
	15 21 47.39	17.66	-1.64	-16.36	-1.34	4.82	138.17	123.01	25.32	88.25	26.13	89.20
	15 21 49.68	1.45	16.23	-0.29	16.44	-0.62	124.91	122.23	25.97	89.01	26.02	89.09
	15 21 52.94	51.13	-21.38	-33.81	-26.53	-36.31	160.44	102.31	22.61	85.49	25.88	88.93
	15 21 56.50	44.38	-18.13	-31.75	-22.01	-32.24	149.12	105.27	23.26	86.00	25.72	88.77
7	15 21 59.86	32.63	-15.86	-29.64	-16.29	-29.93	139.93	117.08	23.94	86.76	25.57	88.61
	15 22 2.64	17.62	-0.15	-14.96	0.36	-15.47	129.34	124.46	24.63	87.55	25.44	88.48
	15 22 4.93	1.42	15.36	-1.61	15.31	-1.62	122.84	121.94	25.28	88.29	25.34	88.37
	15 22 8.19	51.12	-23.79	-36.42	-30.53	-47.85	162.50	103.96	22.11	84.81	25.19	88.22
	15 22 11.75	44.39	-20.86	-33.44	-23.86	-34.27	151.07	107.33	22.56	85.32	25.03	88.06
8	15 22 15.11	32.66	-13.87	-27.64	-14.03	-27.65	142.04	120.16	23.24	86.07	24.88	87.90
	15 22 17.89	17.65	0.10	-15.08	0.49	-15.41	138.58	124.32	23.94	86.85	24.75	87.77
	15 22 20.19	1.45	14.49	-2.12	14.58	-2.48	122.64	122.64	24.59	87.59	24.65	87.67

TABLE 4 (Continued) (DOY 162).

Scan Numb	GMT (Hr Min Sec)	Angle of Incidence (Deg)	Scattering Coefficients VV (DB)	VH (DB)	HH (DB)	HV (DB)	Antenna Temps V (Deg)	H (Deg)	Field of View Coordinates Lat (Deg)	Long (Deg)	Subsatellite Coordinates Lat (Deg)	Long (Deg)
	15 22 23.44	51.15	-22.43	-33.59	-27.97	-37.85	162.21	104.39	21.40	84.14	24.50	87.52
	15 22 27.00	44.42	-17.95	-21.73	-11.92	-16.71	201.83	144.85	21.85	84.64	24.34	87.35
9	15 22 30.36	32.68	-15.08	-29.11	-15.36	-29.93	142.07	128.98	22.54	85.38	24.19	87.20
	15 22 33.14	17.68	0.68	-14.38	0.89	6.58	131.30	125.47	23.24	86.16	24.06	87.07
	15 22 35.44	1.48	14.46	-2.03	14.50	-2.64	122.51	122.06	23.80	86.89	23.96	86.97
	15 22 38.69	51.18	-19.71	-31.85	-24.76	-35.29	162.07	104.41	20.69	83.47	23.81	86.82
	15 22 42.25	44.45	-20.17	-33.43	-23.92	-35.18	150.38	105.24	21.14	83.97	23.64	86.66
10	15 22 45.61	32.71	-13.97	-18.85	-9.79	-14.84	198.02	160.63	21.83	84.71	23.49	86.51
	15 22 48.39	17.71	0.19	-14.64	0.57	-15.45	131.20	124.00	22.54	85.47	23.36	86.38
	15 22 59.69	1.50	13.76	-2.75	13.91	-3.28	124.18	123.29	23.20	86.20	23.26	86.29
	15 22 53.94	51.21	-17.93	-32.18	-23.73	-33.17	161.41	104.01	19.97	82.82	23.11	86.13
	15 22 57.50	44.48	-16.63	-30.59	-20.28	-32.36	152.13	107.65	20.43	83.31	22.95	85.97
11	15 23 0.86	32.74	-14.59	-28.64	-15.54	-29.37	141.53	121.32	21.12	84.04	22.79	85.82
	15 23 3.64	17.72	-1.17	-15.28	-1.46	-13.87	190.13	154.14	21.83	84.80	22.66	85.70
	15 23 5.94	1.52	14.42	-2.53	14.34	-2.92	125.06	122.36	22.50	85.51	22.56	85.60
	15 23 9.19	51.22	-20.08	-32.97	-25.03	-36.32	162.42	103.94	19.25	82.16	22.41	85.45
	15 23 12.75	44.48	-16.45	-29.58	-19.95	-31.32	151.80	107.66	19.72	82.65	22.24	85.29
12	15 23 16.11	32.73	-12.97	-26.43	-13.69	-27.31	144.18	122.57	20.41	83.38	22.09	85.15
	15 23 18.89	17.72	0.51	-14.56	0.61	6.17	133.62	126.26	21.12	84.13	21.96	85.02
	15 23 21.19	1.51	13.86	-3.35	13.74	-3.29	193.95	168.62	21.79	84.84	21.86	84.92
	15 23 24.44	51.22	-25.72	-41.01	-31.27	-39.60	160.36	100.27	18.54	81.52	21.70	84.78
	15 23 28.00	44.47	-20.37	-33.36	-23.33	-37.95	149.53	105.25	19.00	82.01	21.54	84.62
13	15 23 31.36	32.73	-12.21	-26.65	-13.12	-29.15	140.50	118.33	19.70	82.73	21.38	84.48
	15 23 34.14	17.71	0.76	-14.21	1.21	-14.75	133.26	127.39	20.41	83.47	21.25	84.36
	15 23 36.44	1.50	13.80	-2.37	14.12	-3.10	124.85	124.40	21.09	84.18	21.15	84.26
	15 23 39.69	51.21	-26.91	-36.02	-31.35	-37.83	159.42	100.30	17.82	80.88	21.00	84.13
	15 23 43.25	44.47	-23.41	-36.05	-27.07	-40.11	148.73	103.17	18.28	81.36	20.83	83.96
14	15 23 46.61	32.72	-14.10	-28.42	-15.15	-29.11	143.27	118.92	18.98	82.08	20.68	83.82
	15 23 49.39	17.71	1.31	-13.97	1.39	-14.30	132.35	125.13	19.70	82.82	20.55	83.70
	15 23 51.69	1.50	13.80	-2.98	13.79	-3.48	125.13	123.77	20.38	83.52	20.44	83.60
	15 23 54.94	51.21	-27.38	-35.37	-33.21	-41.01	158.97	100.30	17.09	80.25	20.29	83.46
	15 23 58.50	44.46	-24.39	-36.21	-27.90	-47.46	149.49	105.27	17.56	80.73	20.12	83.30
15	15 24 1.86	32.72	-16.87	-30.58	-18.03	-32.26	139.11	116.09	18.26	81.44	19.96	83.16
	15 24 4.64	17.70	0.55	-14.60	1.07	6.18	130.08	123.31	18.98	82.17	19.83	83.04
	15 24 6.04	1.49	-34.30	-33.66	-34.53	-33.16	126.13	124.67	19.66	82.86	19.73	82.94

REFERENCES

1. Moore, Richard K., "Radar Return From The Ground," The University of Kansas Publications, The Bulletin of Engineering, no. 59, 1969.

2. Cook, A. C., Arun Sobti, "Development of an Algorithm for Evaluating the Scatterometer Illumination Integral," CRES Technical Memorandum 236-1, The University of Kansas Center for Research, Inc., Lawrence, Kansas, February, 1973.

3. Hanley, Walter, Ph.D. Thesis, CRES Technical Report 190-2, The University of Kansas Center for Research, Inc., Lawrence, Kansas.

4. Barton, "Radar System Analysis," Appendix C.

5. Barton, "S-193 Microwave Radiometer/Scatterometer Altimeter Calibration Data Report Flight Hardware, Volume 1A," RevD, March 22, 1973.

STATEMENT OF

Dr. Richard K. Moore
Professor of Electrical Engineering
Director, Remote Sensing Laboratory

The University of Kansas

TO

Subcommittee on Manned Space Flight
of the
Committee on Science and Astronautics
U. S. House of Representatives

20 February 1974

Mr. Chairman and members of the committee:

The opportunity to discuss briefly with you some early results, consequences, and implications of the Skylab microwave experiments is a great pleasure and privilege. These experiments have been successful, as nearly as we can tell at this stage. Particular credit should go to those who devised a solution to the antenna problem that developed toward the end of the second manned mission and to the crew of the third mission who made a repair that enabled us to get some outstanding measurements during January.

The success of the Skylab Radscat experiment is particularly gratifying to me, for the Radscat concept was developed by my colleagues Prof. Willard Pierson of City University of New York, Prof. Fawwaz Ulaby of The University of Kansas, and myself. The altimeter experiment also means much to me; although it was developed by Mr. Joseph McGoogan of NASA Wallops Station and colleagues at Naval Research Laboratory and Research Triangle Institute, it is a major step forward in the field where I started in radar in 1951.

The Radscat, which I shall discuss in detail, has demonstrated that a future operational worldwide oceanic wind-measuring satellite system is feasible. We also expect the overland measurements will yield much valuable information required for the design of future spacecraft imaging radars. These will be of value in many applications in disaster monitoring, hydrology, agriculture, and oceanography. The altimeter experiment has shown feasibility of satellite measurement of small vertical changes in the mean sea level, and has gathered much information necessary to produce extremely precise altimeters in the future.

The microwave instruments on Skylab are the S-193 and S-194, with the former being much more complex and versatile. The S-193 operates at a frequency of 13.9 GHz, or wavelength of 2.16 cm. The Radscat portion of the instrument contains a radar scatterometer that measures the strength of a signal that originates in its transmitter, travels to the ground, is scattered (bounced) back to the spacecraft, and is received there. Since all factors except the ground scattering properties are known, the signal strength is a measure of these properties. The radiometer, which shares many receiver components with the scatterometer, measures the strength of microwave "noise" signals that originate in the ground and the atmosphere; its output is expressed as a temperature, but it really is determined both by the temperature and by other properties of ground and air. The altimeter experiment also uses many of the same components, plus some of its own. As an altimeter it measures the distance from spacecraft to ocean very accurately—the situation over land is more complicated. Many of its functions, however, are intended to establish the properties of signals received by an altimeter to permit better design of future systems.

The S-194 is a radiometer operating at a longer wavelength, 21.4 cm (frequency of 1.4 GHz). Like the radiometer in the Radscat, it measures "noise" signal strengths from the ground, but the atmosphere is essentially transparent at its wavelength.

S-193 Oceanographic Applications

The major purpose of the S-193 is oceanographic; measurements over land are important but subsidiary to the oceanographic use. I shall only touch briefly on the altimeter results and concentrate on the Radscat, for my personal involvement is with the Radscat.

One of the first altimeter measurements was over the well-known Puerto Rican trench, an area of the ocean where the mean surface dips sharply because of a very deep spot just off the coast of Puerto Rico. Here is the trace obtained in that measurement. Note that the sea level dips by 14 yards over a relatively short distance. Such a measurement, made in seconds with S-193, is extremely difficult and time consuming when made from ships. This was tried first because it has been well mapped from ships, but other exciting features have been observed in less-well-mapped areas.

The S-193 Radscat was intended to answer questions about the potential of future operational systems to be used continuously over the world's oceans. Its applications to meteorology include measuring ocean-surface winds on a worldwide basis and determining areas of precipitation falling on the sea. Present pictorial weather satellites are used to measure winds at cloud-top level, but the surface winds are also needed to permit better weather forecasts over the sea. From this information better forecasts will be possible over the adjacent land masses as well; and the knowledge gained will permit more knowledge of the physics of the atmosphere, which leads to still better forecasts of the world's weather. Measuring precipitation areas at sea is brand new—we simply have too few ships to make any useful measurements of this kind. This, too, will allow better forecasts and better knowledge of the physics and climatology of the exchange of moisture and heat between air and oceans.

In oceanography, the winds on the surface are the inputs to computer programs used to forecast the waves. Forecasts are now possible in some parts of the Northern oceans where many ships can radio wind speeds to weather centers, but they will be greatly improved by obtaining more input data from satellite Radscats. An operational satellite wind sensor will allow the first forecasts in the Southern oceans where many of the supertankers operate, but the number of ships is too small for adequate forecasting today. These improved wave forecasts will allow faster ship crossings with less damage to cargo and ships, and with the loss of fewer ships. Hence, it will also reduce the chance for major oil spills from damaged or destroyed ships. Fishing industry efficiency can be improved, and better warnings can be made of impending storm hazards along coastlines.

To illustrate the contrast between the present and potential wind data bases, Prof. Pierson has here contrasted the weather map for the South Atlantic on 18 January 1968 as prepared from the sparse available data with what it might be with an operational Radscat. The circles on the left-hand map show the few reporting stations—an occasional ship and coastal stations in Africa and Antarctica. The numbers on the right-hand map show the information that would be available from a single pass of a Radscat on a satellite. The contrast is apparent!

The Radscat concept for an operational wind sensor involves use of a combined radiometer-scatterometer, like that on the S-193 but simpler because of the many modes built into S-193 to answer questions needed for designing the operational system. It would be designed to provide points about 100 km apart on a 1600 km swath—800 km to either side of the satellite ground track. Under clear-sky conditions, both instruments measure windspeed and they may be used to check each other. When the pictorial satellite shows the presence of clouds, the scatterometer is still used to measure wind speed; but the radiometer is more sensitive to the clouds, so it can be used to determine the amount the cloud reduces the signal for the scatterometer; hence, the scatterometer wind measurement may be improved. If the radiometer signal indicates that heavy rain is present, the scatterometer signal is considered too corrupted, and that particular point can be discarded.

All of these concepts were demonstrated early in the first Skylab mission when measurements were made over Hurricane Ava off the Pacific coast of Mexico. This unusual spring storm was observed by Prof. Pierson, who persuaded the flight controllers to modify the flight plan somewhat so this unique opportunity could be

utilized. Mr. Arun Sobti of The University of Kansas calculated how this could be done even without going into the earth-pointed mode. Results of this cooperative effort are shown here. Note the way the wind and scatterometer response follow each other. The one extremely high point for both instruments is an example of the heavy rain condition when the radiometer tells us to disregard the scatterometer indication.

Some results of two passes across the Gulf of Mexico and the Caribbean Sea during the first mission, and of Hurricane Ava, are combined here to show that the horizontally polarized scatterometer signal is approximately proportional to the square of the wind speed. The scatter in the experimental points is believed due in large measure to inadequate knowledge of the winds; we expect that a curve made only with points for which the wind speeds are really well known would show much less scatter, but the amount of scatter shown here would not prevent the data from being of great value to wave forecasting. Note that these measurements were in an area where winds are relatively well known compared with most of the open oceans.

On January 4 of this year we obtained measurements over perhaps the greatest North Atlantic storm of the decade. Here is Prof. Pierson's analysis of this storm. Note that many data points were obtained in winds exceeding 60 knots, with a full range down to relatively low wind speeds. Attempts to obtain aircraft measurements with high winds have been made year after year by both NASA and NRL, but only 2 or 3 points near 50 knots have been obtained, and none near 60 knots! You can imagine how anxious we are to get our hands on the data from this pass!

Let me summarize the significance of the Skylab wind measurement findings to date. First, and to my mind foremost, the Radscat concept works! We have shown that the scatterometer can determine windspeed, the radiometer can correct it in light rain and clouds, and the radiometer can pinpoint heavy rain cells where the data must be discarded. Nevertheless, some factors still must be evaluated to obtain the desired precision of wind measurement; a detailed analysis of the Skylab data should resolve many of these questions. In addition, this analysis will allow pinpointing needs for additional aircraft and tower measurements. Some of these, by the way, may be forthcoming in the underflights made with NASA aircraft using the Radscat developed for aircraft under the AAFE program at NASA Langley Research Center under Dr. W. L. Jones—and this instrument should be the basis for future flights to answer remaining questions. Another significant finding is that we believe our original recommendation for use of vertically-polarized radiation will be changed to horizontal polarization.

S-193 and Spacecraft Imaging Radar

Over land the S-193 is more important in collecting design information for imaging radars than as a test of an operational sensor, for it is not intended to make images like this one from an aircraft sidelooking radar. Yet this kind of detailed picture is needed for many land applications. Just as ERTS with its 200-foot-resolution pictures has been more useful in many applications than the coarser-resolution weather satellites, a spacecraft imaging radar will be more useful over land than S-193—yet S-193 provides valuable information for designing and for some applications of such a sensor.

Radar sensors that can make pictures like this from space are going to be especially valuable for applications where timing is important—where you cannot wait for the clouds to clear before getting a picture. Some examples of these applications are: disaster monitoring and assessment, hydrology, agriculture and other vegetation monitoring, and oceanic applications where images are necessary. Clearly the time to assess a disaster is during or immediately after, even if it is cloudy; this applies to earthquake and volcano damage, to determining the extent of flooding and the damage after the water recedes, to finding out the extent of hurricane and other storm damage, and to pinpointing major oil spills on lake, river, or sea. Forecasting river levels and crop potentials depends on monitoring the moisture stored in the spring snow pack and its changes. Soil moisture has an effect on the flood threat too, as well as on other needs such as keeping track of ground-water levels, but you have to know it at a certain time. Also important for flood forecasting is knowing where the ground is frozen so a rapid melt will run off instead of soaking in, and you have to know the frozen area when the melt starts, not on a later clear day. Irrigation conditions and natural soil moisture are ephemeral. Crops can be best identified by monitoring at the right time in their growth cycle, and this is important if improved forecasts are to be made of yields. The progress of the planting and harvesting cycle can only be monitored while it happens; and plant stresses must be detected early if corrective measures are to be of any use.

Navigation through sea ice requires knowledge that is timely—and so does avoidance of icebergs. If we wish to keep track of fishing fleets and of shipping, we cannot wait for the clouds to go away. Even if we can get the wind forecast from the Radscat, monitoring the wave structure is important in some places; I was told that determining when a certain kind of wave was coming around England from the

North Atlantic might save $500,000,000 in dredging for the channel from Rotterdam to the North Sea!

All of these applications may be possible with spacecraft imaging radars, along with many others not so time-dependent. Many could be handled with other imaging sensors; but, as you can see from this map showing the number of times ERTS photos were possible during the first year of its operation, repeated coverage with photographic and infrared sensors on a schedule is not feasible over much of the country. This is not to say that the ERTS is not useful; ERTS photographs have been of immense value for many applications where timing is not so important, for applications where timing is important in less-cloudy areas, and under fortuitous circumstances for time-dependent applications. Before the ERTS was launched, who would have thought it could find a cloud-free time to map the Amazon jungle? But it did. Nevertheless, operational time-dependent applications will really depend on the cloud-penetrating capability of radar.

How does S-193 fit into this picture since it is not an imaging radar? We already know how to use radar images for many purposes: mapping geological structure, determining the extent of flooding, identifying fields (but not necessarily which crop is there), checking the progress of planting and harvesting, and mapping the extent of sea ice. Radars developed for the DOD have been used commercially for geology, vegetation mapping, and similar applications. The Coast Guard is about to start operational oil-spill radar monitoring near harbors, and the Soviets are routinely mapping sea ice.

Nevertheless many more experiments are needed to determine feasibility of some of the applications suggested here but not yet proven. We do not know yet the best wavelengths and polarizations for different applications—and which ones take combinations of several wavelengths and polarizations. For most uses we do not know just how much ability to discriminate small differences the radar should have. Many of these can be determined with radars mounted on "cherry picker" trucks and on aircraft, but others will require use of the first spacecraft imaging radars. But I still haven't said where Skylab fits!

The data we have obtained with Skylab S-193 will allow us to set the sensitivity of the space radars. Power consumption is very important for these systems since many spacecraft have limited power, and without these data we would be forced to use more power—to be more conservative than necessary. Furthermore we need to know how strong a signal must be accommodated, for the design of the radar system

depends not only on the weakest signal, but also on the range of signal strengths. Even with the rather gross resolution of the S-193, we can find out how well space systems can perform in measuring things that extend across large areas. For example, we are trying to see what success we will have in monitoring regional soil moisture. With coarse resolution, the snow pack in the mountains may be hard to measure, but we can try it in the plains and from this estimate how well a finer resolution system will do in the mountains too. Clearly the advance of the freeze-thaw line is a regional effect that we should be able to monitor from Skylab. Furthermore large homogeneous vegetation stands (for instance, "Texas pastures" or major forests) can be monitored and the results extrapolated to smaller ones that the future fine-resolution radars will map. All of this is in terms of what we will do, because analysis of this kind of data proceeds slowly, and results are not yet available to show.

In one pass across the U.S. on 24 January, however, data were collected from an area so large that this one pass alone will give more information than years of aircraft programs have provided!

Since much of this information will be used for future spacecraft imaging radars, I thought it appropriate to give my ideas of some of the characteristics of systems that we can expect in the near future. All of these systems will perform in clouds and light rain, and some longer-wavelength systems will be independent of rain altogether. Small spacecraft will be restricted to one or two single wavelengths, and resolutions will be in the 30-50 meter range, only a little better than ERTS. In fact the radars may be combined with relatively simple visible-IR sensors with comparable resolutions.

The shuttle or other large spacecraft, however, will be able to carry polypanchromatic radars (true "color" radars with multiple broad-bandwidth capabilities like color film or IR scanners). These systems will have the same kind of advantages over the smaller systems that color photography has over black and white. They will also have better resolution, probably 10-20 meters, although even better is theoretically possible if you could figure out what to do with all the data! These fine-resolution color radars will be combined with equally-fine-resolution high-performance cameras and scanners to provide the best possible all-weather sensing capability. Data collected with S-193 will help bring this about, and we will all benefit from the increased knowledge of our planet that results.

Conclusion

In conclusion, the Skylab microwave systems point toward future operational systems to apply to the needs of man. Already the ability of a spaceborne radar altimeter to profile the ocean surface has been demonstrated; and valuable design information has been collected to permit even better future spacecraft altimeters. The concept has been verified of using a Radscat as a wind-speed sensor for the global oceans, with the radiometer providing corrections to the scatterometer. The Radscat has collected valuable data for design of future imaging spaceborne radars—and for future radiometers, too, although this has not been discussed.

As always, answering some questions raises others. These can, we hope, be answered by further analysis of Skylab data over the next 2 or 3 years, by future space missions, and by continuing aircraft and ground measurements under the NASA S.R.&T. program.

Thank you very much.

WIND DATA BASE CONTRAST

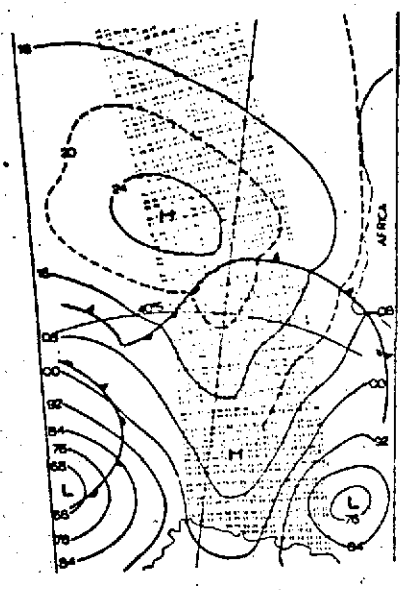

Revised surface analysis for 18 Jan. 1968 based on hypothetical RADSCAT coverage shown. Numbers represent wind speed in knots on a gird like that for expected coverage.

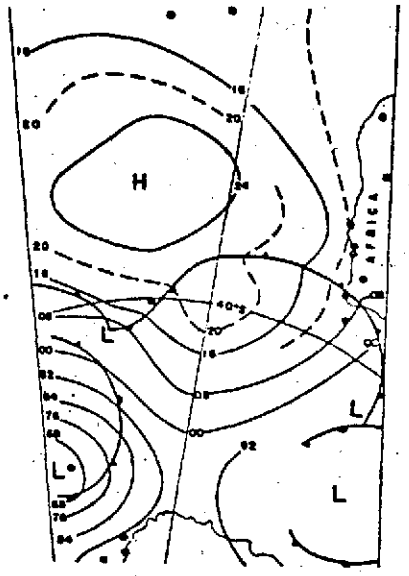

Part of U.S. National Meteorological Center southern hemisphere surface analysis, 18 Jan. 1968. Analysis based on satellite cloud mosaics, surface observations (shown by dots), and continuity.

THE UNIVERSITY OF KANSAS
SPACE TECHNOLOGY CENTER

NASA HQ ML74-5167
2-6-74

SKYLAB ALTIMETER PRELIMINARY DATA RESULTS IN THE ATLANTIC/PUERTO RICO AREA

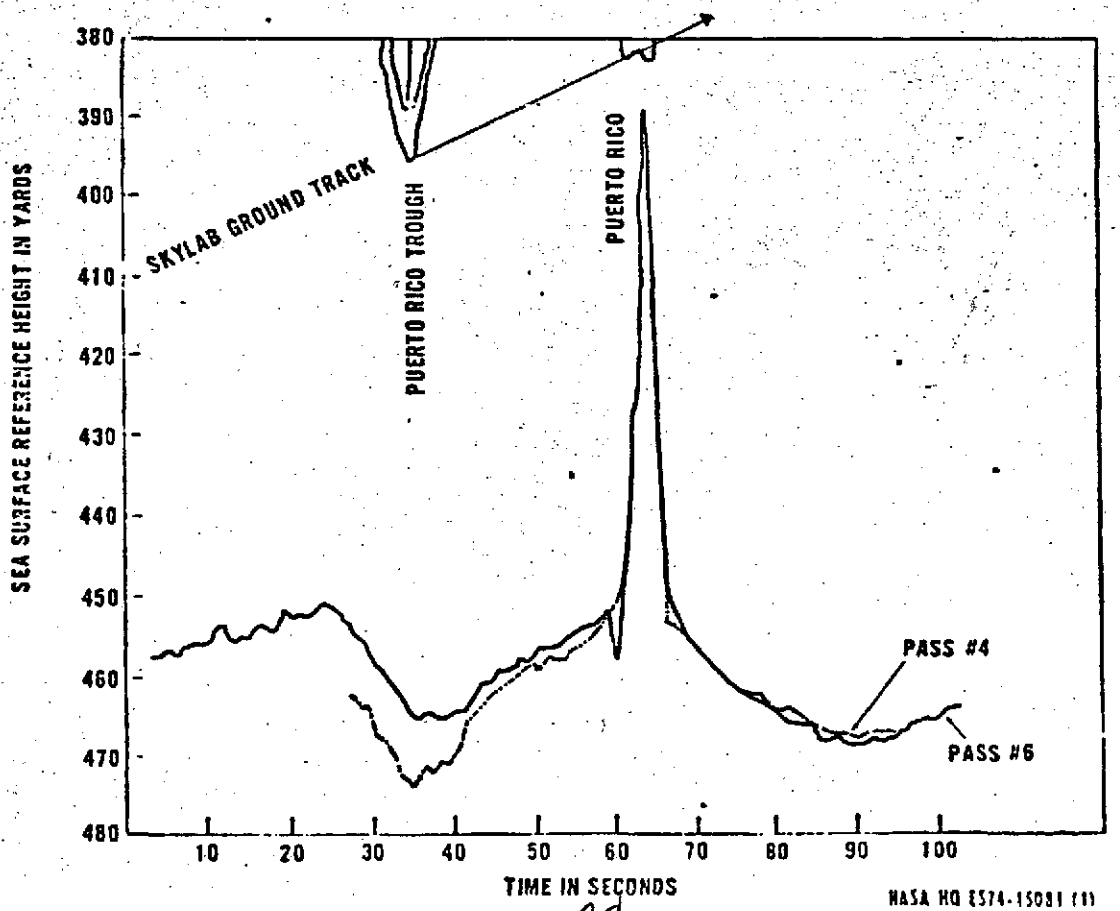

NASA HQ E574-15081 (1) 7/31/73

RESPONSE OF SCATTEROMETER AT 52° OVER HURRICANE AVA

(ASPECT ANGLE AND CLOUD LOSS CORRECTIONS)

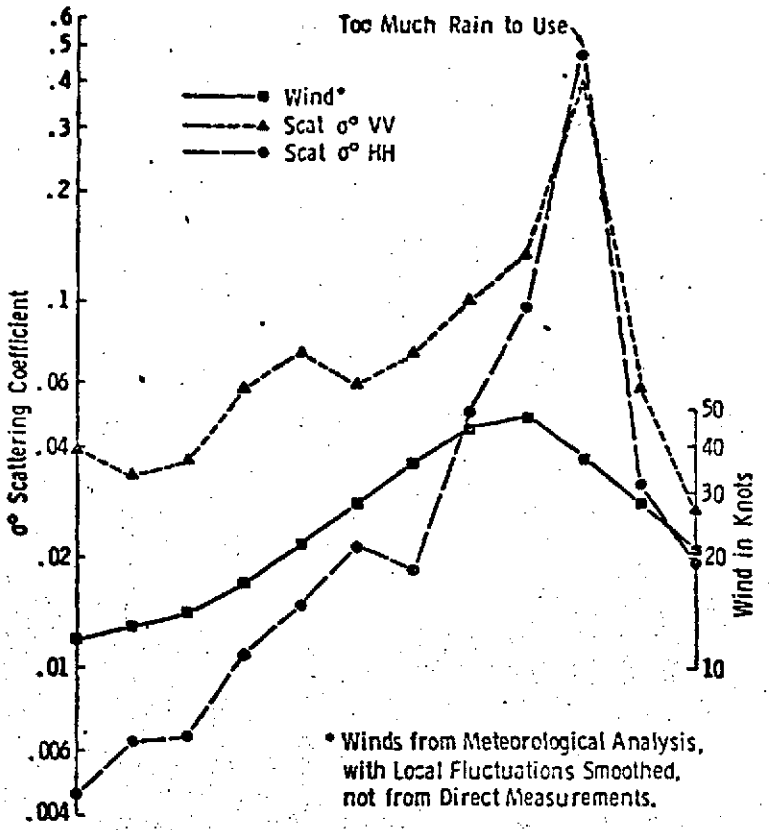

* Winds from Meteorological Analysis, with Local Fluctuations Smoothed, not from Direct Measurements.

THE UNIVERSITY OF KANSAS SPACE TECHNOLOGY CENTER

NASA HQ ML74-5166
2-6-74

S-193 SCATTEROMETER RESPONSE TO WIND AT SEA

3 DAYS IN FIRST SKYLAB MISSION

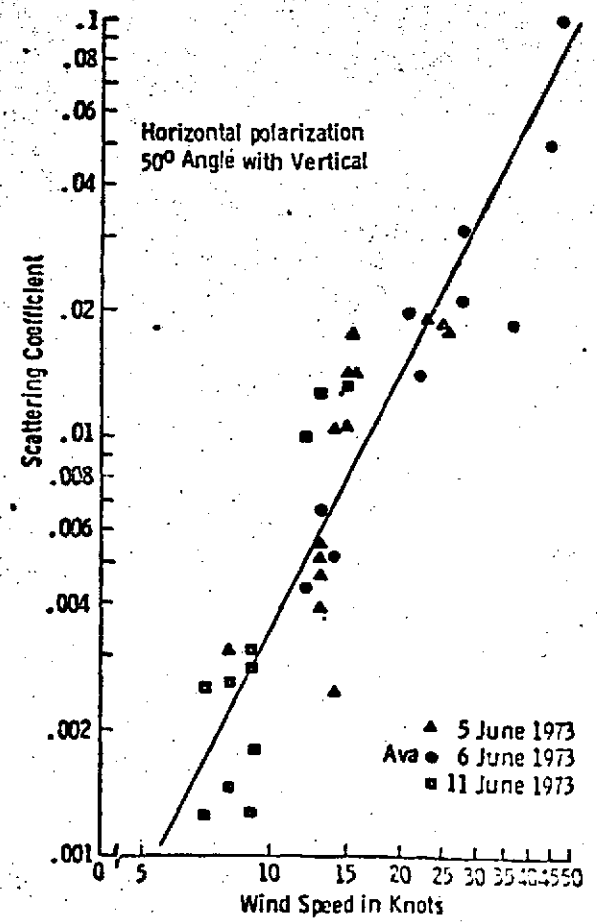

THE UNIVERSITY OF KANSAS SPACE TECHNOLOGY CENTER

NASA HQ ML74-5165
2-6-74

NORTH ATLANTIC SURFACE METEOROLOGICAL ANALYSIS FOR JAN. 4, 1974

S-193 RADSCAT COVERAGE SHOWN FROM NEWFOUNDLAND TO SPAIN

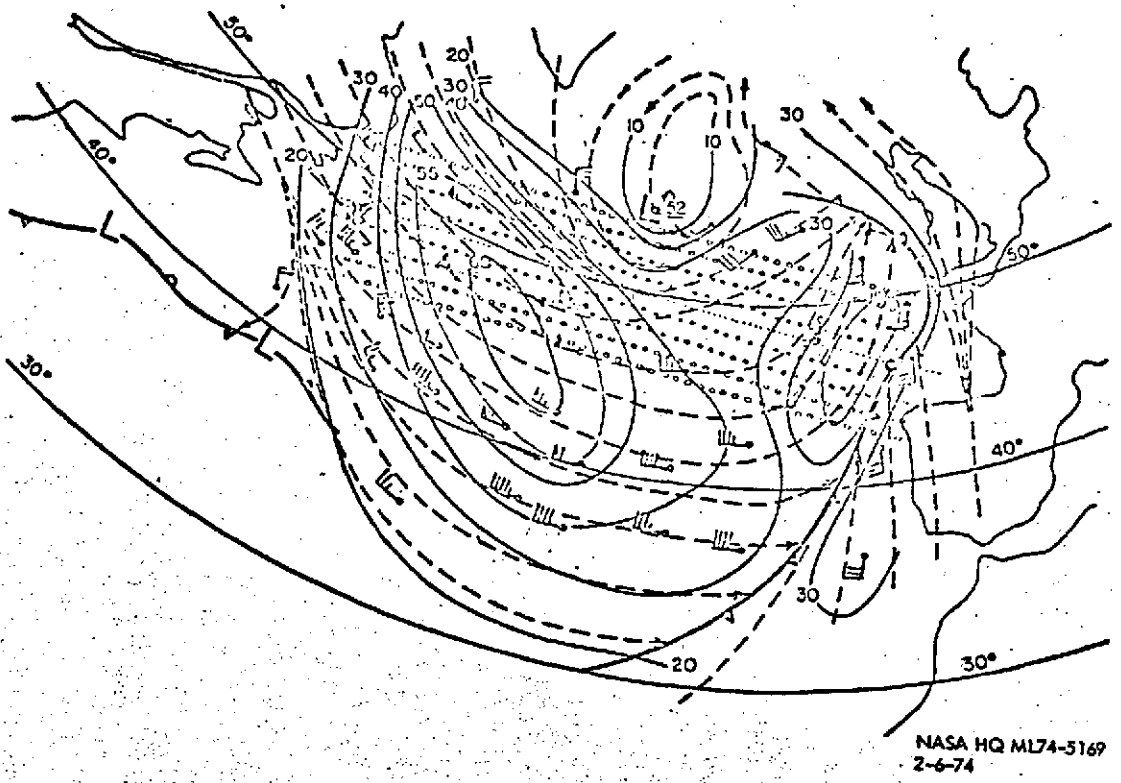

RADSCAT COVERAGE OVER U.S. ON JAN. 24, 1974

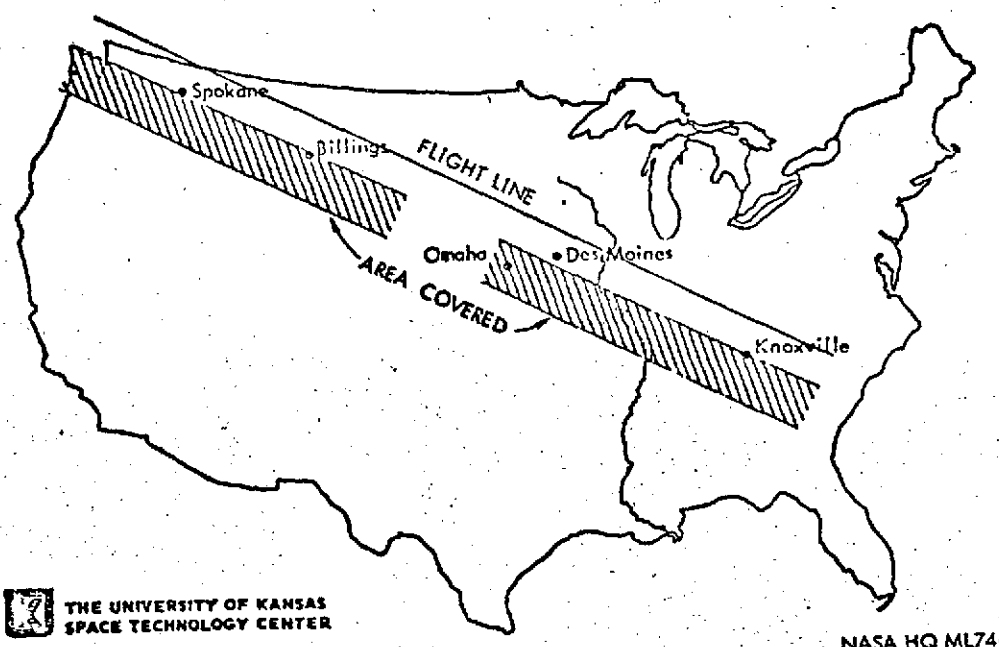

THE UNIVERSITY OF KANSAS
SPACE TECHNOLOGY CENTER

NASA HQ ML74-5168
2-6-74

ERTS 1 CLOUD-FREE COVERAGE

CYCLES 0 - 20 (UNITED STATES) **CLOUD COVER 0 - 30 %**

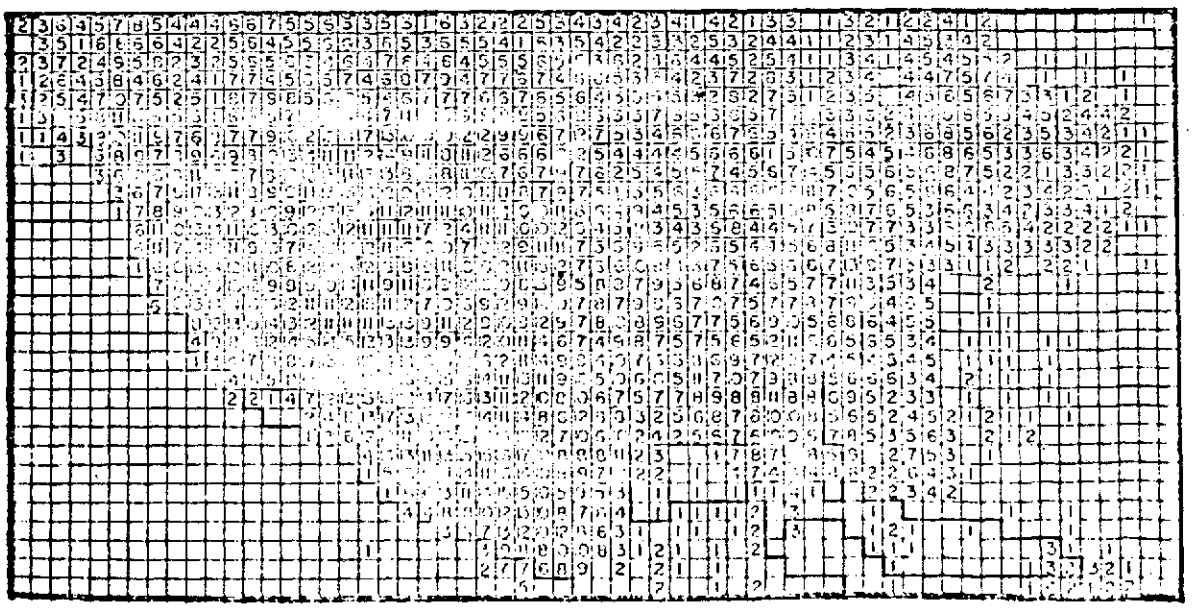

NASA HQ ML74-5206
2-6-74

EARTH — RESOURCES